Made available through Montana State University's ScholarWorks

Long-term water migration in hydrated corn stalk pith and hemp stalk by 250 MHz NMR relaxometry and diffusometry

Matthew C. Young; Sarah L. Codd; Joseph D. Seymour

Accessibility Disclaimer:

For a more accessible version of this document, please submit an accessibility request form through the Montana State University Library website.

Journal of Magnetic Resonance Open 25 (2025) 100210

Contents lists available at ScienceDirect

Journal of Magnetic Resonance Open

journal homepage: www.sciencedirect.com/journal/journal-of-magnetic-resonance-open

Research article

Long-term water migration in hydrated corn stalk pith and hemp stalk by 250 MHz NMR relaxometry and diffusometry

Matthew C. Young [a], Sarah L. Codd [b], Joseph D. Seymour [a,*]

[a] Department of Chemical and Biological Engineering, Montana State University, Bozeman, 59717, MT, USA
[b] Department of Mechanical and Industrial Engineering, Montana State University, Bozeman, 59717, MT, USA

ARTICLE INFO

Keywords:
Lignocellulosic biomass
Nuclear magnetic resonance
NMR relaxometry diffusometry
Pore size distribution

ABSTRACT

Plant fibers are of current interest in biocomposites and known hydrophilicity of plant fibers, e.g. corn stalk pith and hemp stalk, require enhanced understanding of water impacts on fiber structure. Water distribution during hydration in these fibers is compared to fibrous cellulose media using nuclear magnetic resonance (NMR) T_2 relaxometry and diffusometry. Measurements were made every 6 h from 3–237 h, or until equilibrium. NMR T_2 measured bound, intermediate bound and macropore water populations at two water mass hydrations. NMR diffusometry measured diffusion coefficients D of mobile water populations in each material. The diffusion coefficient D was acquired as a function of molecular migration time Δ to detect restricted diffusion. $D(\Delta)$ behavior indicated increased interpore connectivity in highly saturated hemp, versus swollen pores saturated pith. $D(\Delta)$ values were fit for surface to volume ratio S/V to determine average pore radius r as a function of hydration. S/V values were paired to T_2 distributions to provide an effective average transverse magnetic surface relaxivity $\bar{\rho}_2$ throughout hydration, which is then used to rescale T_2 distributions as pore size distributions. Bound water was found in pores < 1 μm, semi-bound water in pores from 1–30 μm and macropore water in pores from 30–300 μm, in agreement with prior literature.

1. Introduction

The strong global push towards sustainability has inspired traditional manufacturing alternatives, including integrating biomass into biocomposite materials [1,2], due plant fiber renewability and low production carbon footprint. However, integrating biomass into composites brings several challenges. First, plant systems are difficult to study due to a complex hierarchy of structures spanning micro, meso and macro scales [3,4]. Additionally, there is a high degree of variability between plant species and even components of the same plant [1,2,5,6]. Underlying this variation are both genetic factors and environmental growing conditions [7], making material specific properties characterization difficult [1]. A final issue with biocomposites is that plant fibers tend to be hydrophilic [1–3], bringing to question their stability in wet and humid conditions. To combat these challenges, much research is focused on characterizing biomass-water interactions, specifically structural rearrangements in wet biomass like swelling [1–3,8]. This study aimed to contribute additional research monitoring long-term water states in saturated and partially unsaturated biomass with nuclear magnetic resonance (NMR) derived pore size distributions (PSD).

Typically in porous media, pores are characterized by PSD. One common method to determine PSD is mercury intrusion porosimetry (MIP), but this technique has limitations. First, mercury is highly toxic. Methods without risk of mercury exposure and mercury waste generation are preferred. Additionally, MIP works by injecting mercury into pore spaces at increasing pressures to probe progressively smaller pores [9], resulting in a high pressure limitation on the minimum pore size measurable [9,10]. High-pressure injections can also damage pore structure and bias measurements [9,10]. Finally, MIP methods are destructive due to mercury injection, so that subsequent characterization on the same sample is impossible.

Another common pore size determination technique, built upon Brunaeur–Emmet–Teller (BET) gas adsorption theory [11] by Barrett, Joyner and Halenda [12], is called BJH [13]. In BJH, inert gas probes the pore structure to provide a PSD [13]. BJH probes surfaces at the molecular scale, and therefore PSD can be dominated by fine features resulting in orders of magnitude higher surface area than other approaches like NMR diffusometry [14]. A second limitation is that BET gas adsorption approaches require a dry sample, potentially problematic when drying induces sample structure changes [14]. Hornification, or drying induced pore collapse, is an established behavior in plant

* Corresponding author.
E-mail address: jseymour@montana.edu (J.D. Seymour).

https://doi.org/10.1016/j.jmro.2025.100210
Received 3 June 2025; Received in revised form 13 August 2025; Accepted 19 August 2025
Available online 4 September 2025
2666-4410/© 2025 The Authors. Published by Elsevier Inc. This is an open access article under the CC BY-NC license (http://creativecommons.org/licenses/by-nc/4.0/).

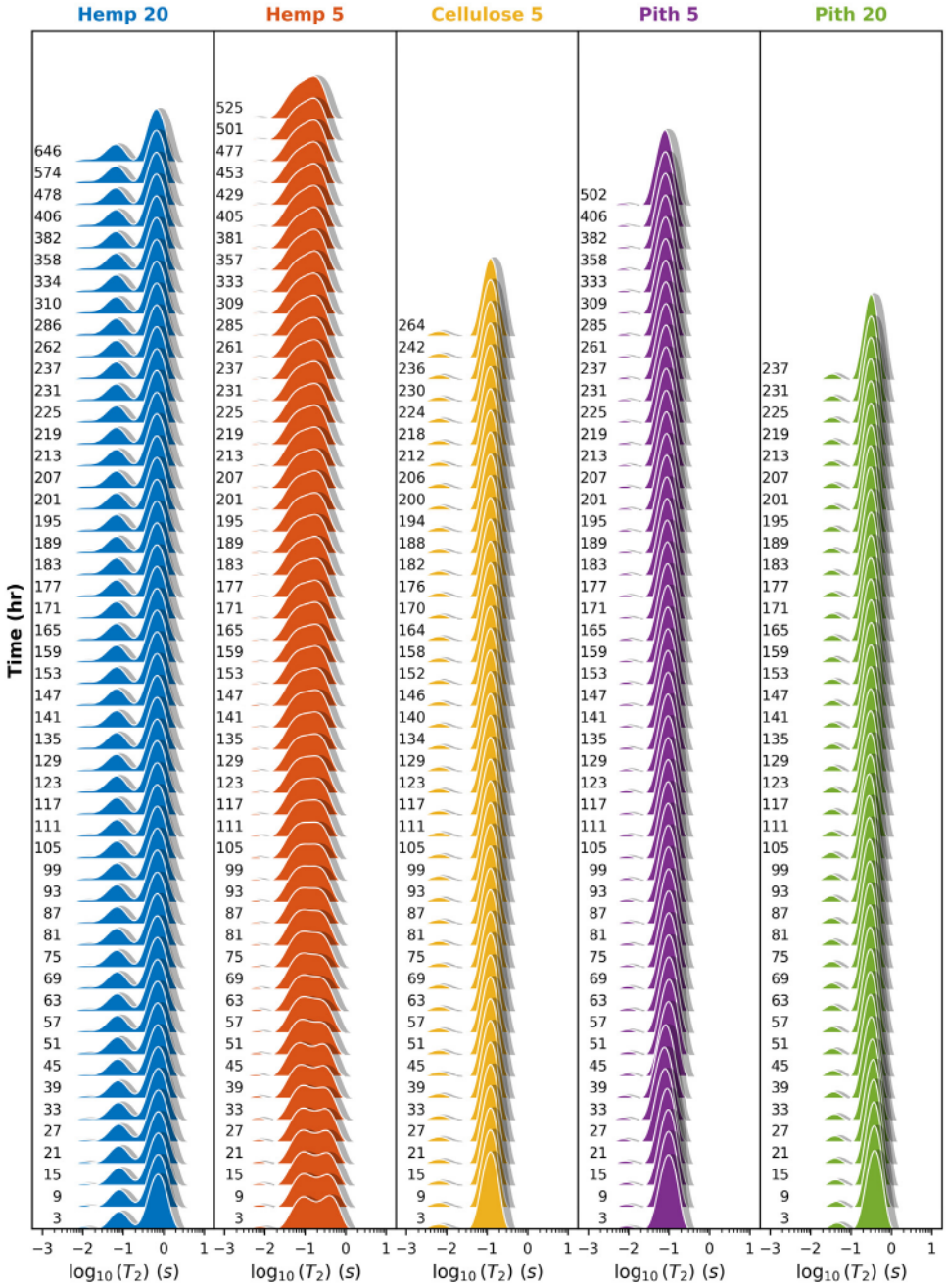

Fig. 1. NMR T_2 relaxation distributions from left to right of hemp stalk at 20 and 5 g_{water}/g_{solid}, fibrous cellulose media at 5 g_{water}/g_{solid}, and corn stalk pith at 5 and 20 g_{water}/g_{solid}. Each material was hydrated, mixed well, loaded into NMR tubes and then monitored until NMR signal ceased to evolve. The numbers on the left of each material panel denotes time after water was added in h. Note that T_2 distributions are offset by an arbitrary amount so that all distributions are visible.

gradually reduces again to $T_2 \sim 80$ ms. Despite these T_2 shifts, there is almost no change in $P(T_2)$ for each population (Fig. 2).

Hemp 5 in Fig. 1 (middle-left column) has a third population at $T_2 \sim 400$ ms. The two mobile populations at $T_2 \sim 100$ and ~ 400 ms are initially the same size and partially merged. By 525 h these populations merge. Before 93 h, $P(T_2)$ of the population at $T_2 \sim 100$ ms grows slightly larger than the population at 400 ms. Beyond 93 h, the most mobile population at $T_2 \sim 400$ ms becomes larger, while simultaneously becoming more restricted. The average T_2 for these populations when merged (Fig. 3) decreases throughout the monitoring period.

Hemp 20 in Fig. 1 (left column) still has three populations. The smallest, highly restricted population, at $T_2 \sim 10$ ms is detected until 310 h. The intermediate mobility population at $T_2 \sim 100$ ms is also detected, but is much smaller than the highly mobile population now at $T_2 \sim 800$ ms. Temporally all three populations shift to shorter T_2, exhibiting decreased system-wide mobility. Over the monitoring period the highly mobile population shrinks while the intermediate mobility population grows, but these changes are less than ±10% (Fig. 2).

Pith 20 in Fig. 1 (right column) initially has a small, restricted mobility, population at $T_2 \sim 50$ ms, and a large, highly mobile, population at $T_2 \sim 400$ ms. From 3–105 h, both populations have reduced mobility, shifting to respective T_2's of ~ 35 and ~ 300 ms (Fig. 3). Beyond 105 h, these populations redevelop some mobility, returning to T_2's of ~ 40 and ~ 350 ms. $P(T_2)$ is nearly constant for each population during the monitoring period (Fig. 2).

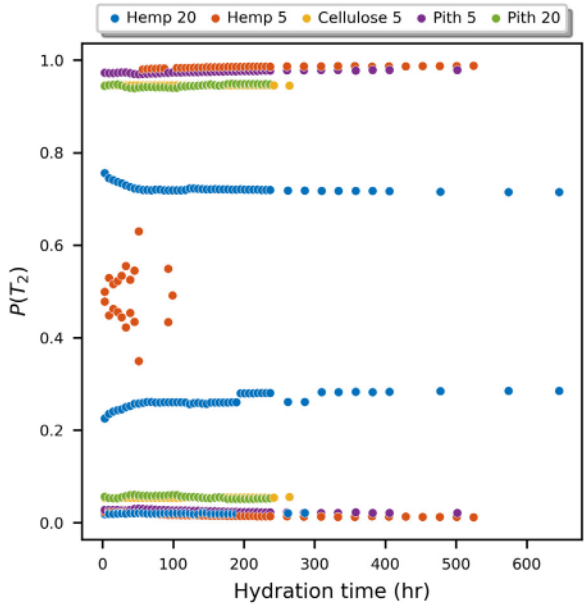

Fig. 2. Changes to peak integrals from Fig. 1 with time. Each peak in Fig. 1 was integrated with Eq. (6) to provide the proportion of signal from each respective domain, indicative of the proportion of ^{1}H in each domain.

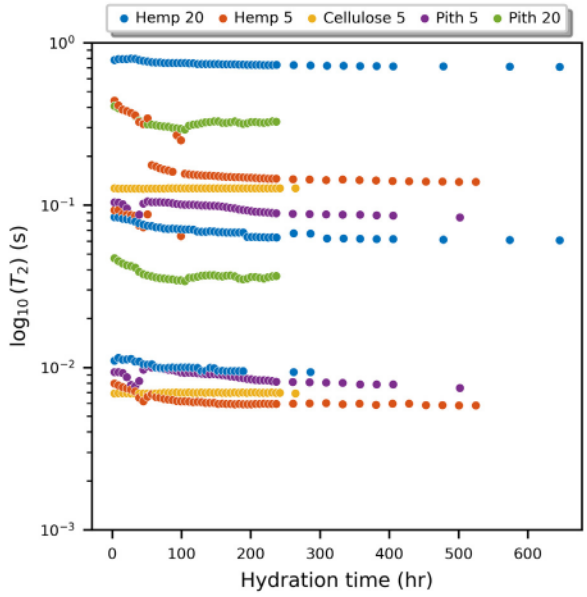

Fig. 3. Changes to average population T_2 from Fig. 1 with time. An average T_2 for each peak in Fig. 1 was calculated with Eq. (7) to provide the average mobility of each domain.

The restricted mobility, bound water, population at short T_2 indicates tightly bound surface associated water in each material at 5 g_{water}/g_{solid} (Fig. 1). The mobile water, population at longer T_2 ~ 100 ms has shorter T_2 than bulk water (~ 3 s), which indicates water-biomass association (Fig. 3). The near order of magnitude longer T_2 of the mobile water over the bound water indicates a much weaker water-biomass association (Fig. 3). Therefore, this mobile population is termed intermediate-bound water as it exhibits loosely bound mobility.

Cellulose 5 shows no temporal change in its two populations, indicating a rapid water-biomass equilibration, without further structural rearrangements or water redistribution. Pith 5 initially has the same two populations at similar T_2 but more water is loosely associated with biomass (Fig. 1 (middle-right column)). The temporal dip in T_2 for pith 5 suggests slow water permeation into the biomass structure so that a greater proportion of water is found tightly associated to surfaces. This additional bound water is presumed to induce structural rearrangements within the biomass, indicated by the partial rebound in T_2.

In hemp 5 (Fig. 1 (middle-left column)) the presence of the most mobile population at $T_2 \sim 400$ ms suggests a saturation of the intermediate-bound 100 ms population. This overflow water is assumed to be macropore water in the fiber bed, and speaks to the low fiber saturation point of hemp fibers compared to cellulose 5 and pith 5. The growth in the intermediate-bound population $P(T_2)$ indicates a slow permeation of macropore water into the 100 msT_2 domain (Fig. 2). Beyond 93 h, the macropore water population begins growing as it merges with the intermediate-bound water domain. As water permeates into the intermediate-bound water domain prior to 93 h, it exerts a hydrostatic pressure on the pore structure. This forces structural rearrangements which increase connectivity and enhancing molecular exchange between the intermediate-bound and macropore water domains. Two plant fiber swelling mechanism have been shown by Garat et al. in which sorption of bound water was observed in addition to macroscopic swelling and structural deformation due to macropore water sorption [2]. It is likely these mechanisms are seen here, with the first dominating before 93 h, and the latter beyond 93 h.

Pith 20 in Fig. 1 (right column) has a restricted water and mobile population with nearly 5x longer T_2 than pith 5. Rather than bound and intermediate-bound water as in pith 5, this mobility in pith 20 is more representative of intermediate-bound and macropore water (Fig. 3). Pith 20 also has a greater restricted water proportion than pith 5 (Fig. 2). $P(T_2)$ for pith 20 matches cellulose 5 (Fig. 2), with longer T_2 values for pith 20, indicating a similar water distribution with larger pore sizes (Fig. 3). $P(T_2)$ does not change in pith 20 because no water migrates between populations, informing minimal interaction between pools of water (Fig. 2). The temporal shift to shorter T_2, followed by partial rebounding indicates biomass structural rearrangements due to hydrostatic pressure from absorbed water (Fig. 3).

In hemp 20 (Fig. 1 (left column)), the highly mobile macropore water population has double the mobility of hemp 5, at $T_2 \sim 800$ ms instead of ~ 400 ms (Fig. 3). As this long T_2 approaches the 3 s T_2 of bulk water, it indicates weakening macropore water-biomass interaction. The temporal T_2 shortening is attributed to loosening of microfibril-bundle packing, increasing interfibrillar water accessibility and overall water restriction. A T_2 rebound, which indicated structural rearrangements in hemp 5, is not observed in hemp 20 due to more rapid water equilibration due from the 4x water increase. The additional water enhances water permeation, so that the following the hydrostatic driven structural rearrangement of fibers is predominantly measured. The temporally increasing intermediate-bound water $P(T_2)$, decreasing macropore water $P(T_2)$, and decreasing T_2 for both domains further supports a long-term fiber rearrangement hypothesis. As water adds to the intermediate-bound domain it strengthens water-biomass interactions on average.

T_2 signal is assumed to only detect water in each system, a good assumption given the order of ~ 10 μs relaxation times of cellulose protons [18]. $P(T_2)$ values in Fig. 4 can then be scaled by the total water mass on a per gram solid basis to estimate the relative water mass water in each domain (Fig. 8). In cellulose 5 the intermediate-bound water mass nearly equals the total water added. The bound water domain is ~ 0.25 g/g. Both hemp 5 and pith 5 have a similar distribution of water to cellulose 5, once the hemp 5 intermediate-bound and macropore water populations merge, with more macropore water than cellulose 5. Hemp 20 has nearly the same amount of water in these two populations, with slightly more bound water. In hemp 20 the extra 15 g/g of water is added as mobile macropore water at $T_2 \sim 800$ ms (Fig. 3). Temporally in Hemp 20 there is some macro pore water migration to the intermediate-bound domain, indicating some

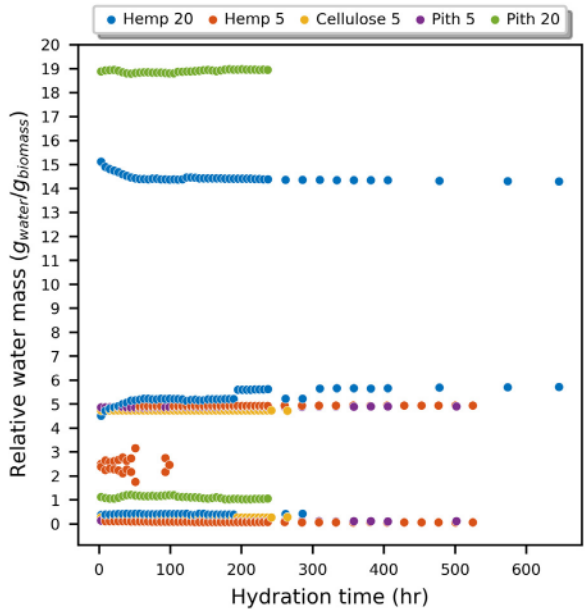

Fig. 4. Integrated $P(T_2)$ for each population from Fig. 2 rescaled to a per mass basis. Assuming all signal comes from water ^{1}H, $P(T_2)$ multiplied by the sample water mass on a per gram solid basis provides the relative mass of water in each population as $P(T_2)m_{watertotal}$.

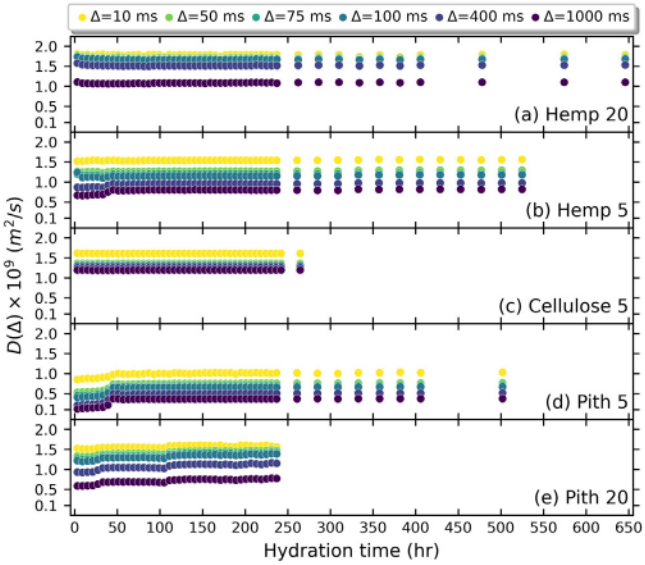

Fig. 5. Results from the most mobile component in NMR diffusometry measurements of (a) 20 and (b) 5 g_{water}/g_{solid} hemp stalk, (c) 5 g_{water}/g_{solid} fibrous cellulose media, and (d) 5 and (e) 20 g_{water}/g_{solid} corn stalk pith. Diffusometry signal attenuation with ramping gradients were fit to estimate the diffusion coefficient D of water in these systems. D values reported are multiplied by 10^9 for readability. In addition, these data were acquired as a function of molecular migration time Δ to inform if time-diffusive dynamics, indicative of restricted diffusion, are present. Points are colored based on Δ, but generally D decreases with increasing Δ in each panel, as expected.

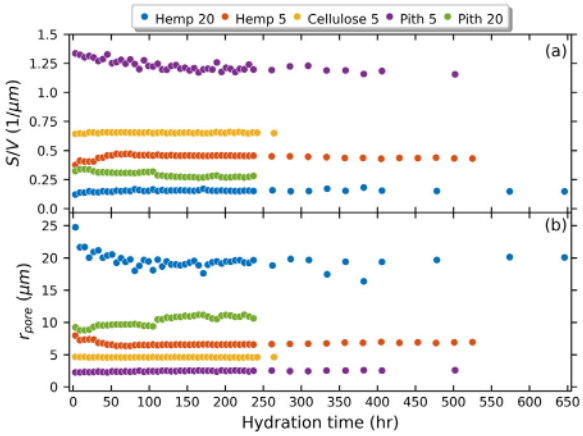

Fig. 6. NMR diffusometry derived (a) surface to volume ratios and (b) pore radius estimates. From a Padé approximation fit (Eq. (3)) to the $D(\Delta)$ data in Fig. 5, S/V was estimated (a). This S/V value was used to estimate pore radius (b) using a spherical pore scaling of $3/r$.

long-time water absorption. Pith 20 uptakes water into both domains, with ~ 1 g/g water in the intermediate-bound domain and ~ 19 g/g in the macropore water domain, informing an impressive hydrostatically increased water storage capability. The increased T_2 in the pith 20 populations (Fig. 3) indicates larger pore sizes, attributed to swelling.

5.2. NMR diffusometry

NMR PGStE results in Fig. 5 are sensitive to the most mobile water populations in these systems. This is why the measured D do not always vary dramatically from the $D = 2 \times 10^{-9}$ m^2/s of bulk water. D was measured as a function of molecular migration time Δ to probe for restricted diffusion. Time-dependent diffusive behavior is uncharacteristic of free molecular self-diffusion, seen as decreasing D with increasing Δ. This inverse proportionality indicates restricted diffusion, where local environments limit molecular diffusion within pores.

D from the most mobile component in NMR PGStE signal (Fig. 5) displays temporal hydration behavior complementary to T_2 relaxation measurements. Cellulose 5 is the least dynamic material, with a slight $D(\Delta)$ dependence but no change over the monitoring period (Fig. 5(c)). Cellulose 5 D values are all between 1.0×10^{-9} m^2/s and 1.7×10^{-9} m^2/s, minimally varying from water molecular self-diffusivity. S/V is highly sensitive to D at short Δ times. The large D drop between Δ = 10 ms and 50 ms, leads to larger S/V fit values from Eq. (3) than hemp 20, hemp 5 and pith 20 (Fig. 6(a)).

Compared to cellulose 5, hemp 5 has a stronger total $D(\Delta)$ dependence, with a greater total spreading of D between 0.6×10^{-9} m^2/s and 1.5×10^{-9} m^2/s (Fig. 5(b)). There is a gradual increase in D for Δ = 100, 400 and 1000 ms data until 50 h. This temporal D increase for the longest Δ informs enhanced interpore migration from improved interpore connectivity.

Pith 5 exhibits a similar temporal change until ~ 50 h (Fig. 5(d)), with $D(\Delta)$ spread initially ranging from 0.1×10^{-9} m^2/s to 0.8×10^{-9} m^2/s. Smaller D values complement T_2 data in Fig. 1 (middle-right) where no macropore water was measured, demonstrating the well established high absorbency of corn stalk pith [44,45]. Stronger water-biomass associations than in cellulose 5 or hemp 5 cause the low D measured. D also increases until 50 h, similar to hemp 5, except D increases across all Δ values suggesting pore swelling and enhanced interpore connectivity. In Fig. 6(a) S/V for pith 5 modestly decreases until 150 h, further supporting a pore swelling interpretation.

Hemp 20 and pith 20 in Fig. 5(a) and (e) have the largest drop in D at long Δ times. Hemp 20 in Fig. 5(a) spans D values from 1×10^{-9} m^2/s and 1.8×10^{-9} m^2/s, with the highest diffusivity, the smallest S/V (Fig. 6(a)) and largest pores (Fig. 6(b)) of all tested materials. This supports the hemp 20 T_2 data which observed highly mobile macropore water. In addition, there is a large drop in D of 0.5×10^{-9} m^2/s between Δ = 400 ms and 1000 ms, likely due to motional narrowing as molecules sample the entire pore space and

rebound off pore walls during the 1000 ms Δ. During the first 20 h of hydration, hemp 20 D decreases for all Δ times. Beyond 20 h, the biomass continues to absorb water, strengthening the water-biomass interaction strength, decreasing diffusivity and increasing S/V (Fig. 6(a)). However, regardless of experiment time, hemp 20 D is still larger than hemp 5 in Fig. 5(b).

The most temporally dynamic material is pith 20, changing through 100 h (Fig. 5(e)). Pith 20 spans $D(\Delta)$ values between 0.5×10^{-9} m^2/s and 1.5×10^{-9} m^2/s, which is the largest range of all materials tested. This spread is dominated by large D drops at long Δ times of 400 and 1000 ms. As with hemp 20 in Fig. 5(a) these large D drops at long Δ support motional narrowing. Total sampling of the pore space by water leads to rebounding off pore walls and decreased effective diffusivity at these long times. Temporally pith 20 increases in D independently of Δ until 30 h. Beyond 30 h D decreases for all data points. Beyond 105 h D again increases and then plateaus. Changing D across all Δ suggests pore structure modification. Coinciding with this temporal evolution, S/V in Fig. 6(a) decreases with time, implying an increase in pore sizes.

Comparing pore radius estimates between materials in Fig. 6(b) informs hydration induced swelling. Note that S/V estimates in this data are subject to some error based on the $\Delta^{1/2}$ linear fits over the sparsely sampled short Δ points. However, these points do show linear trends. Also, spherical pores are assumed here so that r scales as $3/(S/V)$, i.e. r directly reflects V/S. At 5 g_{water}/g_{solid} hemp 5 has the largest pores between 6.0–8.0 μm, cellulose 5 is lower at 5.0 μm and pith 5 is around 2.5 μm. At 20 g_{water}/g_{solid}, hemp 20 has the largest radius of 19.0–25.0 μm. The jump between hemp 5 and hemp 20 once equilibrated, i.e. at long hydration times, is 13 μm or 3.2x larger. Pith 5 jumps from 2.5 to ~ 9–11 μm in pith 20, an equilibrated increase of 8.5 μm or 4.4x larger. Hemp 5 has the largest r of all the 5 g_{water}/g_{solid} samples, indicating that it has already undergone swelling and is closest to saturation. Further swelling in hemp 20 is not proportional to the 4 times increase in water. Continuing with the spherical pore assumption, the change in pore volume scales as $(r_{final}/r_{inital})^3$. Hemp's increase in r from 6 to 19 μm leads to a volume increase of ~ 32x. Pith's r increase from 2.5 to 11 μm is an impressive ~ 85x increase in pore volume. This massive water absorptivity and swellability are established characteristics of corn stover [6] and specifically corn stalk pith [44,45].

5.3. Surface relaxivity

Empirical effective $\bar{\rho}_2$ values enable conversion from T_2 distributions to PSDs [37], setting up routine T_2 relaxation measurements for characterization and quality control in biocomposite manufacturing. The question with this approach is how to best use the T_2 data. An averaged T_2 for the entire distribution can determine the average $\bar{\rho}_2$ which is assumed to be uniform across the sample. An alternative approach assumes $\bar{\rho}_2$ is not constant across all pore sizes, requiring $\bar{\rho}_2$ determination for each water pool or $\bar{\rho}_{2,i}$. This approach requires matching S/V for each pool of water with its average T_2 [46], requiring $D-T_2$ correlation experiments at each Δ; an intensive and difficult approach for temporally evolving systems due to increased experiment durations. Due to the need to minimize total NMR experimental acquisition times, to mitigate the effects of water migration during each experimental set, these authors have elected to instead use an averaged T_2 from each T_2 distribution (Fig. 1) with a bulk PGStE derived S/V (Fig. 6(a)) to estimate $\bar{\rho}_2$ for the entire system at each time point (Fig. 7). $\bar{\rho}_2$ relates T_2 distributions in Fig. 1 directly to PSDs in Fig. 8 using Eq. (4). However, note that because the PGStE derived S/V values in Fig. 6(a) are from the fastest diffusing component in the signal decay these PSDs will be biased towards the largest pores. The reported PSDs are likely skewed to larger pores than the actual distribution of pore-sizes.

Effective surface relaxivity $\bar{\rho}_2$ values derived for these materials (Fig. 7) are temporally dynamic as structural rearrangements either alter surface chemistry [47] or open up volume relaxation sinks with water solubilized biomolecules [39], an interesting result in itself. These values are not constant in time for hemp 5, hemp 20, pith 5 and pith 20. Cellulose 5 $\bar{\rho}_2$ is nearly constant throughout hydration. This temporal nature in the biomass requires a calibration curve of $\bar{\rho}_2$ versus hydration time to estimate PSDs from T_2 relaxation. Using the same $\bar{\rho}_2$ value across all time points would not accurately reflect the changing biomass-water interaction. The effective $\bar{\rho}_2$ still has units of a surface reaction sink μm/s and as such is an average magnetization surface reaction flux term in the model, but now reflects both magnetization loss along surfaces and in the pore fluid [48]. Interactions with paramagnetic species or long surface water adsorption times leads to greater magnetic relaxation along surfaces and increased $\bar{\rho}_2$. Additionally the effective surface relaxivity term is increased by volume sinks, in which mixtures of water and biomolecule solutes lead to reduced overall T_2 of the pore water [38]. In hydrated biomass, a $\bar{\rho}_2$ increase can be caused by longer water adsorption times, indicating stronger water-biomass surface interactions and increased affinity for water within cellulose microfibrils. In addition, solubilization of complex polysaccharides such as pectins, proteins and other biomolecules with leakage of cytoplasm into the surrounding water can be causes of volume sink effects in plants, similar to the effects seen in muscle [39]. T_2 NMR relaxation data has previously been related to mercury intrusion porosimetry (MIP) to calculate $\bar{\rho}_2$ in the lumen of wood cells [10]. These results show $\bar{\rho}_2$ scales with pore size, and report $\bar{\rho}_2 = 64$ μm/s in cell lumen pores and $\bar{\rho}_2 = 2.7$ μm/s in cell wall pores [10]. Therefore, the long-time increase in $\bar{\rho}_2$ for each material in this work, except cellulose 5, indicates larger pore sizes. This continued swelling is caused by water induced structural rearrangements, increasing water affinity and promoting additional water uptake.

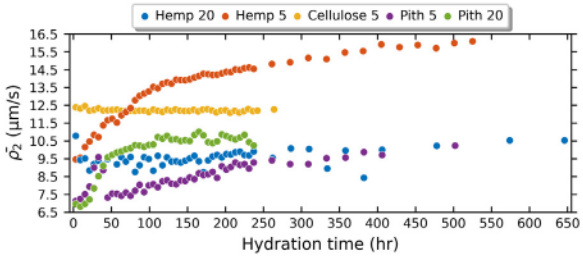

Fig. 7. Average surface relaxivity $\bar{\rho}_2$ calculated from T_2 NMR data in Fig. 1 and NMR diffusometry derived S/V data in Fig. 6(a) with Eq. (4) at each hydration time point. These results clearly show that $\bar{\rho}_2$ is not constant during these hydration experiments in each material except cellulose 5.

T_2 distributions in Fig. 1 are converted to PSDs in Fig. 8 using Eq. (4) with $\bar{\rho}_2$ from each hydration time point in Fig. 7. These distributions show pore sizes ranging from 0.1 and 300 μm. The 5 g_{water}/g_{solid} materials have a small water population in pores ~ 0.2–0.5 μm, while the majority of water is in pores between 1–10 μm for cellulose 5 and pith 5 and 1–50 μm for hemp 5. At 20 g_{water}/g_{solid}, hemp 20 has pores below 1 μm, between 1–10 μm and between 10–300 μm. Pith 20 has pores ~ 1 μm and 3–30 μm. These results are in good agreement with other pore-size characterization techniques on different lignocellulosic materials. In dry wood lumens MIP showed a small proportion of pores below 1 μm, along with major pore populations at roughly 1, 10 and 100 μm [10]. In dry corn stalk, MIP has measured PSDs with a small number of pores at 1 μm, along with various larger pores ranging from 10 μm and 300 μm [21]. In sugarcane bagasse, SEM images showed water in cell walls of 2–5 μm thickness, narrow lumens of 10 μm and wide lumens of 70 μm [20]. These results confirm the PSDs reported in Fig. 8 are scaled to the correct order of magnitude.

6. Conclusion

This study investigated long-term hydration in pith, hemp and cellulose using NMR T_2 relaxometry and diffusometry. Pith and hemp

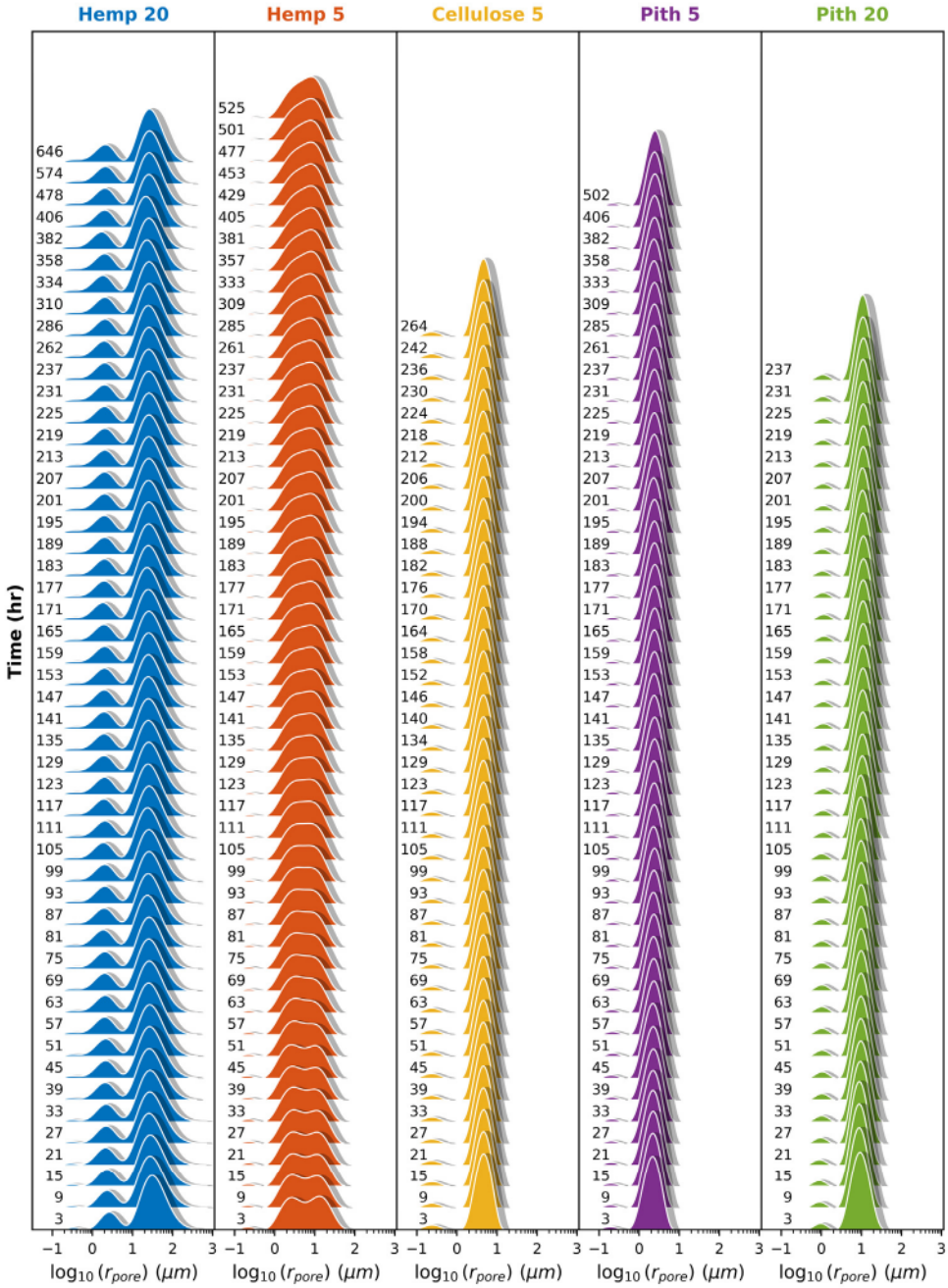

Fig. 8. PSDs derived from surface relaxivity $\bar{\rho}_2$ in Fig. 7 and NMR T_2 relaxation distributions in Fig. 1. Note the high degree of similarity between these distributions and Fig. 1 is because T_2 distributions essentially represent rescaled PSDs. Here the T_2 scaling has been adjusted to reflect the water-containing-PSD in these samples, using the approach outlined in the text.

were monitored at 5 and 20 g of water per g of solid, and cellulose was monitored at 5 g of water per g of solid. All materials were measured every 6 h until 237 h, after which measurement frequency was decreased until no change was observed. T_2 relaxation detected bound and intermediate-bound water in cellulose 5 and pith 5. Hemp 5 had bound, intermediate-bound and macropore water, indicating saturation of the restricted sites by 5 g of water per g biomass. Pith 20 displayed high absorptivity as all water was absorbed during the 237 h hydration time. The additional 15 g of water between hemp 20 and hemp 5 added as macropore water. NMR diffusometry measured diffusion coefficients D of the most mobile water populations in each material. All values were within an order of magnitude of D for bulk water. D was acquired as a function of molecular migration time Δ to probe for restricted diffusion. The $D(\Delta)$ behavior showed increased interpore connectivity in hemp 20, and swollen pores in pith 20. These $D(\Delta)$ values were used to estimate S/V and an average pore size r of each sample. S/V values were paired with T_2 distributions to provide effective transverse surface relaxivity $\bar{\rho}_2$ estimates as a function of hydration time. $\bar{\rho}_2$ varied with hydration time, as surface properties and biomolecule concentration in solution in pore water evolved. $\bar{\rho}_2$ was used to rescale T_2 distributions to pore size distributions at each observed time point. Bound water was found to be in pores < 1 μm.

[32] P.P. Mitra, P.N. Sen, L.M. Schwartz, P. Le Doussal, Diffusion propagator as a probe of the structure of porous media, Phys. Rev. Lett. 68 (24) (1992) 3555–3558, http://dx.doi.org/10.1103/PhysRevLett.68.3555.
[33] P.N. Sen, Time-dependent diffusion coefficient as a probe of geometry, Concepts Magn. Reson. A 23a (1) (2004) 1–21, http://dx.doi.org/10.1002/cmr.a.20017.
[34] L.L. Latour, P.P. Mitra, R.L. Kleinberg, C.H. Sotak, Time-dependent diffusion coefficient of fluids in porous media as a probe of surface-to-volume ratio, J. Magn. Reson. A 101 (3) (1993) 342–346, http://dx.doi.org/10.1006/jmra.1993.1056.
[35] J.E. Tanner, Use of the stimulated echo in NMR diffusion studies, J. Chem. Phys. 52 (5) (1970) 2523–2526, http://dx.doi.org/10.1063/1.1673336.
[36] M.D. Hurlimann, L.L. Latour, C.H. Sotak, Diffusion measurement in sandstone core: NMR determination of surface-to-volume ratio and surface relaxivity, Magn. Reson. Imaging 12 (2) (1994) 325–327, http://dx.doi.org/10.1016/0730-725x(94)91548-I.
[37] R.L. Kleinberg, Utility of NMR T2 distributions, connection with capillary pressure, clay effect, and determination of the surface relaxivity parameter rho 2, Magn. Reson. Imaging 14 (7–8) (1996) 761–767, http://dx.doi.org/10.1016/s0730-725x(96)00161-I.
[38] Kenneth R. Brownstein, C.E. Tarr, Importance of classical diffusion in NMR studies of water in biological cells, Phys. Rev. A 19 (6) (1979) 2446, http://dx.doi.org/10.1103/PhysRevA.19.2446.
[39] Kathryn E. Anderssen, Evan R. McCarney, Mechanisms of transverse relaxation of water in muscle tissue, Food Control 132 (2022) http://dx.doi.org/10.1016/j.foodcont.2021.108373.
[40] Y.Q. Song, L. Venkataramanan, M.D. Hurlimann, M. Flaum, P. Frulla, C. Straley, T(1)–t(2) correlation spectra obtained using a fast two-dimensional Laplace inversion, J. Magn. Reson. 154 (2) (2002) 261–268, http://dx.doi.org/10.1006/jmre.2001.2474.
[41] L. Venkataramanan, Y.Q. Song, M.D. Hurlimann, Solving fredholm integrals of the first kind with tensor product structure in 2 and 2.5 dimensions, IEEE Trans. Signal Process. 50 (5) (2002) 1017–1026, http://dx.doi.org/10.1109/78.995059.
[42] S. Godefroy, P.T. Callaghan, 2D relaxation/diffusion correlations in porous media, Magn. Reson. Imaging 21 (3–4) (2003) 381–383, http://dx.doi.org/10.1016/s0730-725x(03)00144-I.
[43] Edmund J. Fordham, Lalitha Venkataramanan, Jonathan Mitchell, Andrea Valori, What are, and what are not, inverse Laplace transforms, Diffus. Fundam. 29 (2017) http://dx.doi.org/10.62721/diffusion-fundamentals.29.952.
[44] C. Igathinathane, A.R. Womac, S. Sokhansanj, L.O. Pordesimo, Sorption equilibrium moisture characteristics of selected corn stover components, Trans. ASAE 48 (4) (2005) 1449–1460, http://dx.doi.org/10.13031/2013.19170.
[45] C. Igathinathane, A.R. Womac, S. Sokhansanj, L.O. Pordesimo, Moisture sorption thermodynamic properties of corn stover fractions, Trans. ASABE 50 (6) (2007) 2151–2160, http://dx.doi.org/10.13031/2013.24075.
[46] M.D. Hürlimann, L. Venkataramanan, C. Flaum, The diffusion-spin relaxation time distribution function as an experimental probe to characterize fluid mixtures in porous media, J. Chem. Phys. 117 (22) (2002) 10223–10232, http://dx.doi.org/10.1063/1.1518959.
[47] Neil Robinson, Razyq Nasharuddin, Einar O. Fridjonsson, Michael L. Johns, NMR surface relaxivity in a time-dependent porous system, Phys. Rev. Lett. 130 (12) (2023) http://dx.doi.org/10.1103/PhysRevLett.130.126204.
[48] J.E. Maneval, M.L. Nelson, L.W. Thrane, S.L. Codd, J.D. Seymour, A two-region transport model for interpreting T1-t2 measurements in complex systems, J. Magn. Reson. 308 (2019) 106592, http://dx.doi.org/10.1016/j.jmr.2019.106592.